Supporting Information

Antibacterial photodynamic inactivation of antibiotic-resistant bacteria and biofilms with nanomolar photosensitizer concentrations

Carolina S. Vinagreiro,[†] Amanda Zangirolami, [‡] Fabio Schaberle,[†] Sandra C. C. Nunes,[†] Kate C. Blanco, [‡] Natalia M. Inada,[‡] Gabriela Jorge da Silva,[#] Alberto A. C. C. Pais,[†] Vanderlei S. Bagnato,[‡] Luis G. Arnaut*,[†] and Mariette M. Pereira*,[†]

[†]Chemistry Department, University of Coimbra 3004-535 Coimbra, Portugal

[‡]São Carlos Institute of Physics, University of São Paulo, 13566-590, São Carlos, São Paulo, Brazil

[#]Faculty of Pharmacy and Center for Neurosciences and Cell Biology, University of Coimbra, 3000-548 Coimbra, Portugal

Index

1. Calculations

Figs. S1 and S2 present the molecular structures of free-base and zinc complexes of cationic porphyrins optimized at the B3LYP/6-31G(d,p) level. **Fig. S3 and S4** present the Mulliken charges free-base and zinc complexes of cationic porphyrins. **Fig. S5 and S6** present the HOMO and LUMO orbitals of free-base and zinc complexes of cationic porphyrins. The electronic densities of porphyrins with *N*-methylpyridinium and 1,3-dimethylimidazolium substituents are presented in the main text. Molar volumes (V_M) and solvent excluded surface areas (SE) are presented in Table 1. Calculations with substituents other than 1,3-dimethylimidazolium were also performed to assess positive charge densities of alternative dicationic photosensitizers of small size. **Fig. S7** and **S8** present their electronic densities. No obvious advantage was found over 1,3-dimethylimidazolium porphyrins.

DFT calculations revealed that 1,3-dimethylimidazolium substituents lead to dihedral angles very close to 90° whereas such angles in porphyrins with *N*-methylpyridinium substituents are much lower, Table 2. This means that the imidazolyl ring is nearly orthogonal to the macrocycle but not the pyridyl ring. The calculations also reveal that hydrogen atoms of the methyl groups bonded to the nitrogen atoms of the imidazolyl ring have a remarkably high positive charge density. For example, for **IP-4-Zn+** the Mulliken charge on such hydrogen atoms are: 0.20, 0.20 and 0.15 for one methyl, and 0.20, 0.15, 0.20 for the methyl on the other side of the macrocycle, and very similar values are found for the other three imidazolyl rings. These hydrogen atoms surround the macrocycle. For **Zn-TMPyP** similar charges are present in the hydrogen atoms of the methyl groups bound to the nitrogen atom of the pyridyl ring: 0.20, 0.20 and 0.19. However, these hydrogen atoms are far from the macrocycle and directed away from it.

2. Experimental Procedures

2.1. General methods

All solvents were dried according to standard procedures. All commercial reagents were purchased from Sigma-Aldrich and Fluorochem and used without further purification. UV–vis spectra were recorded on Hitachi U-2001 or Shimadzu 2100 spectrophotometers using spectroscopic grade solvents. The ^{1}H and ^{13}C NMR spectra were recorded on a 400 Bruker Avance spectrometer (400 and 101 MHz, respectively), using tetramethylsilane (δ = 0.00 ppm) as internal standard for ^{1}H and ^{13}C. The multiplicity is indicated as follows: s - singlet, sl - large singlet, d - doublet, t - triplet, q - quartet, dd - double doublet, m – multiplet. The electrospray ionization (ESI) mass spectra were obtained at the Mass Spectrometry Unit (UniMS), ITQB/iBET, Oeiras, Portugal. Confocal microscopy images were acquired using a Zeiss

fluorescence confocal microscope (LSM 780 inverted model) with laser excitation (LASER Diode 405 nm). The microscope was equipped with high sensitivity GaAsP detectors for spectral imaging (400-700 nm). Some photoinactivations employed a light source designed and built at the Laboratory of Technical Support of the São Carlos Institute of Physics, São Paulo University, named Biotable®. It is composed by 24 LED lamps that deliver a light fluence rate at 30 mW/cm² of uniform irradiation in the wavelength range between 400-650 nm.

2.2. Synthesis and characterization

Scheme S1: Preparation of 5,10,15,20-(1,3-dimethylimidazol-2-yl) porphyrinate zinc (II) tetraiodide **IP-4-Zn+**

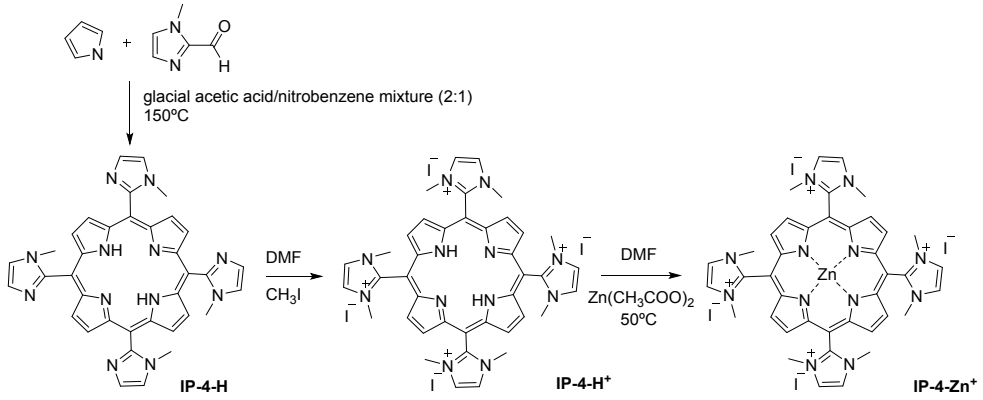

Preparation of the precursor 5,10,15,20-(1-methylimidazol-2-yl)porphyrin, (IP-4-H). IP-4-H was synthesized accordingly to some modifications of previously described nitrobenzene methodology.[1-2] In a typical experiment, 1-methylimidazole-2-carboxaldehyde (4.73 g, 43 mmol) is introduced into a 250 mL flask and a glacial acetic acid/nitrobenzene mixture (140 mL/70 mL) is added, followed by drop wise addition of equimolar amount of pyrrole (3 mL, 43 mmol), under stirring, at T = 150 ºC. The solution was maintained at 150 °C for 2 h. After cooling, the solvents were removed by low-pressure distillation and the remaining solid was dissolved in dichloromethane. The tetra-imidazolyl-porphyrin **IP-4-H** was purified by silica gel column chromatography using first dichloromethane and finally dichloromethane/methanol (10:1) as eluents. The solvents were evaporated and the solid **IP-4-H** was dried under vacuum. Yield = 14% (1.04 g). ^{1}H NMR (400 MHz, $CDCl_3$): δ mixture of atropoisomers 8.91-8.86 (sl, 8H), 7.69 (dd, J = 1.3, 5.7 Hz, 4H), 7.49 (dd, J = 1.4, 3.2 Hz, 4H), 3.55-3.38 (sl, 12H), -2.84 to -2.95 (sl, 2H). UV-vis (CH_2Cl_2): λ_{max}/nm (log ε): 420 (5.31), 513 (4.14), 552 (sh), 587 (3.67), 658 (3.59). The data is in agreement with the literature,[3] **(Fig. S9 and S10).**

Preparation of the precursor 5,10,15,20-(1,3-dimethylimidazol-2-yl) porphyrin tetraiodide, (IP-4-H+). The quaternization of imidazolyl groups of **IP-4-H** (0.0793 mmol, 50 mg) was achieved *via* quaternization of nitrogen atoms with a large excess of iodomethane (7.93 mmol, 0.494 mL) in DMF (0.2 mL) at 30 ºC, along 24 hours. The evolution of the reaction was followed by TLC. The product **IP-4-H+** was precipitated with diethyl ether and, after filtration, almost quantitative yield was obtained**.** ^{1}H NMR (400 MHz, DMSO-D_6, 25°C): δ 9.32 (s, 8H), 8.54 (s, 8H), 3.76 (s, 24H), -3.21 (sl, 2H). UV-vis (H_2O): λ_{max}/nm (log ε): 407 (5.22), 507 (4.17), 541 (3.73), 579 (3.79), 630 (3.78). The data is in agreement with the literature,[4] **(Fig. S11 and S12)**.

5,10,15,20-(1,3-Dimethylimidazol-2-yl) porphyrinate zinc (II) tetraiodide, (IP-4-Zn+). 5,10,15,20-(1,3-dimethylimidazol-2-yl) porphyrin tetraiodide **IP-4-H+** (20 mg; 0.0167 mmol) was dissolved in DMF (5 mL) and zinc acetate (30.6 mg; 0.167 mmol) was added. Then, the solution was kept at 50 ºC under stirring. The complexation was monitored by UV-Vis until the Soret band change from 407 to 417, the 4 Q bands disappeared and two new bands at 556 and 586 nm appeared. After completion of the reaction, the desired porphyrin was precipitated with a mixture of dichloromethane and diethyl ether, dissolved in water and the excess of zinc acetate was removed in a Sephadex G10 column chromatography. After purification, 19.4 mg (92% yield) of **IP-4-Zn+** was obtained. ^{1}H NMR (400 MHz, DMSO-D_6, 25°C): δ 9.23 (d, J = 8.8 Hz, 8H), 8.52 (d, J = 9.4 Hz, 8H), 3.70 (d, J = 8.7 Hz, 24H). UV-vis (H_2O): λ_{max}/nm (log ε): 417 (5.43), 556 (4.23), 586 (4.03). The data is in agreement with the literature,[5] **(Fig. S13 and S14).**

Note 1: The zinc (II) complex should be prepared after cationization of the imidazole group to avoid the formation of polymeric aggregation in solution with a typical band around 480 nm as previously described.[6]

Characterization of 5,15-bis(1,3-dimethylimidazol-2-yl)porphyrinate zinc (II) diiodide (IP-2-H), 5,15-bis(1-methylimidazol-2-yl)porphyrinate zinc (II) (IP-2-Zn), and 5,15-bis(1,3-dimethylimidazol-2-yl)porphyrinate zinc (II) diiodide, (IP-2-Zn+).

^{1}H NMR Spectra, UV-vis spectra, ESI mass spectra of the title compounds are presented in **Figures S15-S22**.

2.3. Molar absorption coefficients

Molar absorption coefficients were determined by using Beer-Lambert's law. For each compound, a minimum of 6 solutions were prepared in concentrations ranging from 10^{-7} to 10^{-6} M, giving absorbance values between 0.1 and 1. **Figure S23** shows representative Beer-Lambert plots

2.4. Partition coefficients

A modification of the shake-flask method was employed to determine the equilibrium concentrations of the photosensitizer in *n*-octanol and in phosphate-buffered saline (PBS), using the typical fluorescence band of the same photosensitizer and calibration curves. Equal volumes of *n*-octanol and PBS are mixed and allowed to stand. The photosensitizer was dissolved in octanol (5 mL) with saturated PBS solution and then saturated PBS with octanol (5 mL) was added thereto. The mixture was stirred vigorously and centrifuged at 3700 rpm. To a volume of 2 mL of the PBS part, pure octanol (0.5 mL) was added. The PBS was evaporated under reduced pressure (about 50 °C) and 2.5 mL of pure octanol was added thereto. On the other hand, to a volume of 2 ml of the octanol part, pure octanol (1 mL) was added to maintain equal dilutions in the organic and aqueous phase. Finally, fluorescence spectra of each of the phases are carried out and the partition coefficient calculated. The logarithms of *n*-octanol:water(PBS) partition coefficients of **IP-4-Zn+** and **IP-2-Zn+** are –1.8±0.4 and –1.16±0.08, respectively, from the average of two independent measurements.

2.5. Fluorescence quantum yields

The fluorescence emission spectra were recorded in a Horiba Scientific Spectrofluorometer Fluoromax-4. The spectra were collected from 550 nm up to 800 nm using standard cuvettes of 1 cm of optical path. Fluorescence quantum yields (Φ_F) were obtained comparing the area of integrated fluorescence of the samples (F_s) with that of a reference (F_{ref}) fluorimetric compound with known Φ_F, corrected by the absorption of sample (A_s) and reference (A_{ref}) at the excitation wavelength and by the refractive index of the solvents used for the sample (η_s) and reference (η_{ref}) solutions

$$\Phi_F = \Phi_F^{ref} \frac{F_s A_{ref} \eta_s^2}{F_{ref} A_s \eta_{ref}^2}$$

Tetraphenylporphyrin (TPP) in toluene ($\Phi_F^{ref} = 0.11$)[7] was used as standard. The absorbance of the solutions at the excitation wavelength was 0.01. **Figure S24** shows representative absorption and fluorescence plots.

2.6. Singlet oxygen quantum yields

The experiments were run at room temperature heavy water (D_2O). **Figure S25** presents representative electronic absorption spectra in D_2O. The solutions were excited at 355 nm using a Nd-YAG laser (Spectra-Physics Quanta-Ray GRC-130) and the phosphorescence of singlet oxygen collected at 1270 nm in a Hamamatsu R5509-42 photomultiplier, cooled to 193 K in a liquid nitrogen chamber, after selection of the wavelength with a monochromator with 600 lines grading. A Newport filter model 10LWF-1000-B was used in the emission to avoid scattering and fluorescence. Phenalenone was used as a reference of singlet oxygen generator, $\Phi_\Delta^{Ref} = 0.98$.[8] Extrapolating to time-zero the decays of the singlet molecular oxygen emissions measured for sample and the reference solutions at a given laser intensity, we obtained a relation between emission intensities as a function of laser intensity, that is identical to the relation between the singlet molecular oxygen quantum yields. **Figure S26** presents representative relations between the time-zero extrapolated singlet oxygen phosphorescence and the relative energies of the laser pulses used to excite the photosensitizer at 355 nm. The singlet oxygen quantum yields were obtained by comparing the linear dependence between singlet oxygen emission and the energy of the laser pulse for both the sample (S_S) and the reference (S_{ref}), for the same absorption of sample (A_S) and reference (A_{ref}) at the excitation wavelength, taking into account the singlet oxygen quantum yield of phenalenone

$$\Phi_\Delta = \Phi_\Delta^{ref} \frac{S_s}{S_{ref}} \frac{1-10^{-A_s}}{1-10^{-A_s}}$$

This equation includes a term to correct for minor differences in absorption at 355 nm.

2.7. Photodecomposition quantum yields

Photodecomposition experiments were made dissolving **IP-4-H+** in water and **IP-2-Zn+** in water with 9% dimethylsulfoxide. A volume V_{irr} = 3 mL was placed in a 1 cm cuvette (l = 1 cm) and irradiated ensuring that all the light went through the solution. The porphyrins were irradiated for a time Δt using a LED light with emission λ = 415 nm and output power P_0 = 0.5 mW. The actual light power absorbed (P) was determined for each compound and properly taken into account in the calculation of the photodecomposition quantum yield.[9] Photodecomposition quantum yield (Φ_{pd}) is defined as the ratio between the rate of disappearance of photosensitizer molecules v_d and the rate of absorption of photons v_P,[10]

$$\Phi_{pd} = \frac{v_d}{v_p} = \frac{V_{irr} N_A hc}{\varepsilon_{506.5} l \lambda_{415} P\left(1-10^{-A_0}\right)} \frac{\Delta A_{506.5}}{\Delta t}$$

where A_0 is initial absorption at the wavelength of excitation.

Photodecomposition may lead to colored products and, at some wavelengths, rather than a decrease in absorbance, an increase may be observed. We found that at 506.5 nm a decrease in absorption was observed for both photosensitizers and followed the photodecomposition at this wavelength. **Figures S27** and **S28** show the spectra and their changes with the illumination time. The spectral changes at 506.5 nm were fit with a linear decay to obtain $\Delta A/\Delta t$, and the following values were obtained: $\Phi_{pd} = 4x10^{-5}$ for **IP-4-H+** in water and $\Phi_{pd} = 8x10^{-6}$ for **IP-2-Zn+** in water with 9% dimethylsulfoxide.

References

1. Gonsalves, A. M. d. A. R.; Varejão, J. M. T. B.; Pereira, M. M., Some new aspects related to the synthesis of meso-substituted porphyrins. *J. Heterocycl. Chem.* **1991,** *28*, 635-640.
2. Monteiro, C. J. P.; Pereira, M. M.; Pinto, S. M. A.; Simões, A. V. C.; Sá, G. F. F.; Arnaut, L. G.; Formosinho, S. J.; Simões, S.; Wyatt, M. F., Synthesis of amphiphilic sulphonamide halogenated porphyrin: Maldi-TOF mass spectra characterization and evaluation of 1-octanol/water partition coefficients. *Tetrahedron* **2008,** *64*, 5132-5138.
3. Tjahjono, D. H.; Akutsu, T.; Yoshioka, N.; Inoue, H., Cationic porphytins bearing diazolium rings: synthesis and their interacion with calf thymus DNA. *Biochem. Biophys. Acta* **1999,** *1472*, 333-343.
4. Maximiano, R. V.; Piovesan, E.; Zílio, S. C.; Machado, A. E. H.; de Paula, R.; Cavaleiro, J. A. S.; Borissevitch, I. E.; Ito, A. S.; Gonçalves, P. J.; Neto, N. M. B., Excited-state absorption investigation of a cationic porphyrin derivative. *J. Photochem. Photobiol. A: Chem.* **2010,** *214*, 115-120.
5. Machado, A. E. H.; Gomes, W. R.; Araújo, D. M. S.; Miglio, H. S.; Ueno, L. T.; de Paula, R.; Cavaleiro, J. A. S.; Neto, N. M. B., Synhesis and spectroscopic chracaterization of two tetrasubstituted cationic porphyrin derivatives. *Molecules* **2011,** *16*, 5807-5821.
6. Kobuke, Y.; Ogawa, K.; Kugimiya, S.-i. Poly(porphyrin) arrays having meso-dimeric imidazolyl porphyrin metal complexes as monomer units. US patent 6429310-B2, 2001.
7. Pineiro, M.; Carvalho, A. L.; Pereira, M. M.; Gonsalves, A. M. d. A. R.; Arnaut, L. G.; Formosinho, S. J., Photoacoustic measurements of porphyrin triplet-state quantum yields and singlet-oxygen efficiencies. *Chem. Eur. J.* **1998,** *4*, 2299-2307.
8. Schmidt, R.; Tanielian, C.; Dunsbach, R.; Wolff, C., Phenalenone, a universal reference compounds for the determination of quantum yields of singlet oxygen. *J. Photochem. Photobiol. A: Chem.* **1994,** *79*, 11-17.
9. Schaberle, F. A., Assessment of the actual light dose in photodynamic therapy. *Photodiagnosis Photodyn. Ther.* **2018,** *23*, 75-77.
10. Silva, E. F. F.; Pimenta, F. M.; Pedersen, B. W.; Blaikie, F. H.; Bosio, G. N.; Breitenbach, T.; Westberg, M.; Breghøj, M.; Etzerodt, M.; Arnaut, L. G.; Ogilby, P. R., Intracellular singlet oxygen

photosensitizers: on the road to solving the problems of sensitizer degradation, bleaching and relocalization. *Integr. Biol.* **2016,** *8*, 177-193.

Table S1. Molar volumes (V_M) calculated with Gaussian, assuming that the volume is defined by a contour of 0.001 e/a_0^3 and solvent excluded surface area (SE) for a probe of radius 1.4 Å.

	IP-4-H+	**IP-4-Zn+**	**IP-2-H+**	**IP-2-Zn+**	**TMPyP**	**Zn-TMPyP**	**DMPyP**	**Zn-DMPyP**
V_M / (cm^3/mol)	511	501	343	375	493	464	342	348
S_E / (Å^2)	590	589	433	431	593	592	435	433

Table S2. Dihedral angles calculated with Gaussian.

Position	**IP-4-Zn+**	**IP-2-H+**	**IP-2-Zn+**	**Zn-TMPyP**	**DMPyP**	**Zn-DMPyP**
5-position	92.2°	-97.3°	82.5°	65.6°	-50.8°	55.0°
10-position	92.7°			69.1°		
15-position	87.2°	103.0°	101.9°	65.4°	50.8°	124.8°
20-position	91.0°			115.0°		

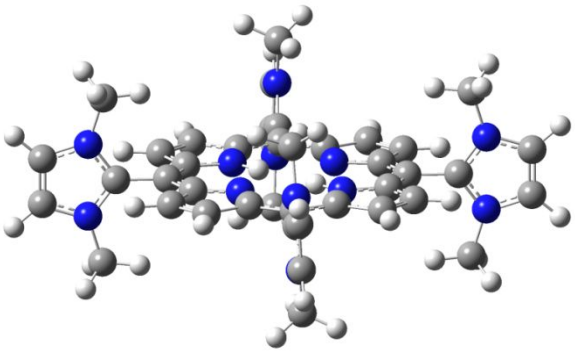

IP-4-H+

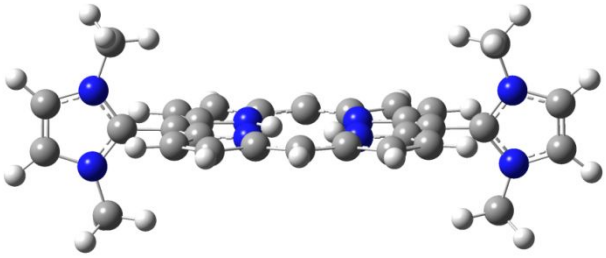

IP-2-H+

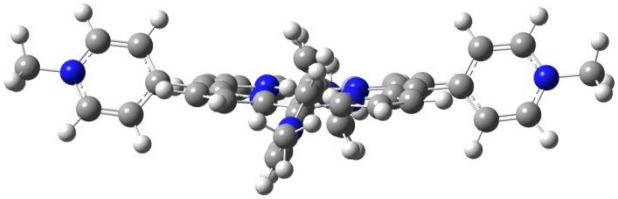

TMPyP

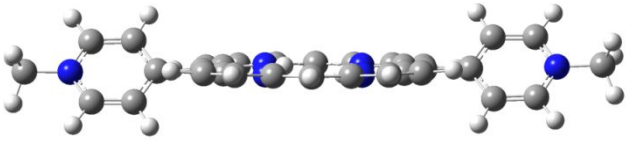

DMPyP

Figure S1. Molecular structures of free-base cationic porphyrins optimized at the B3LYP/6-31G(d,p) level.

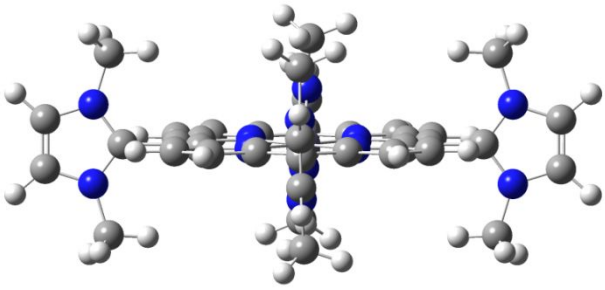

IP-4-Zn+

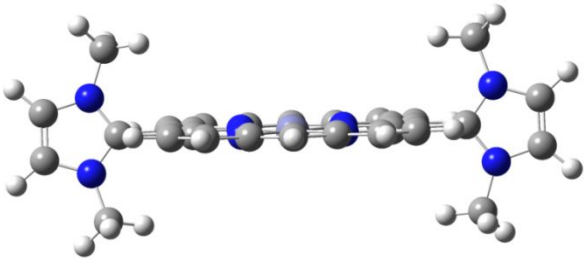

IP-2-Zn+

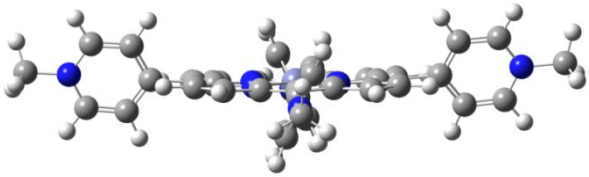

Zn-TMPyP

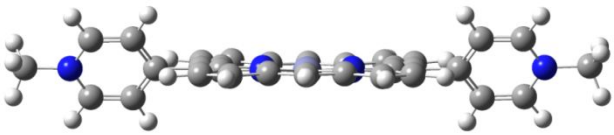

Zn-DMPyP

Figure S2. Molecular structures of zinc complexes of cationic porphyrins optimized at the B3LYP/6-31G(d,p) level.

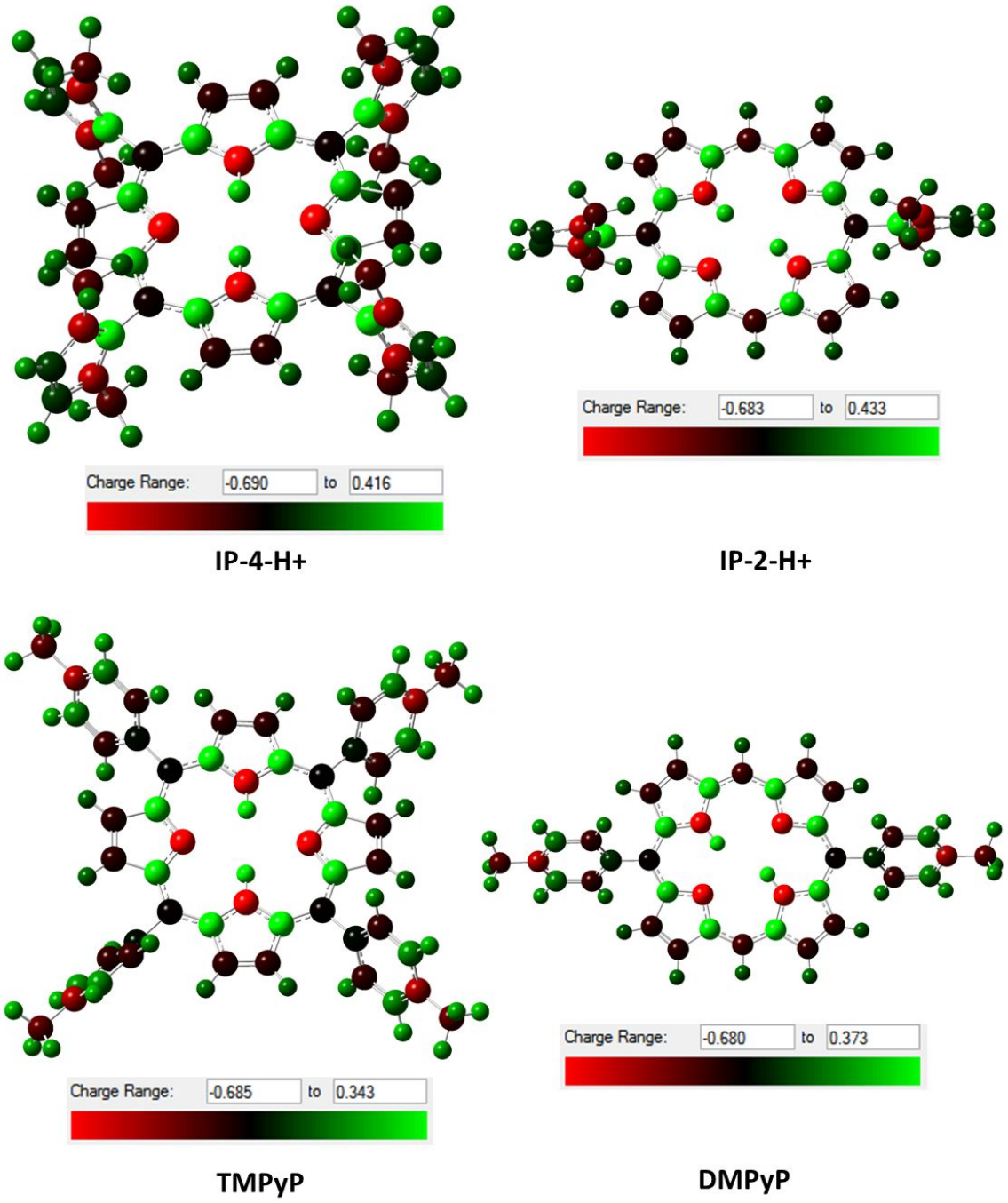

Figure S3. Mulliken charges of free-base cationic porphyrins optimized at the B3LYP/6-31G(d,p) level.

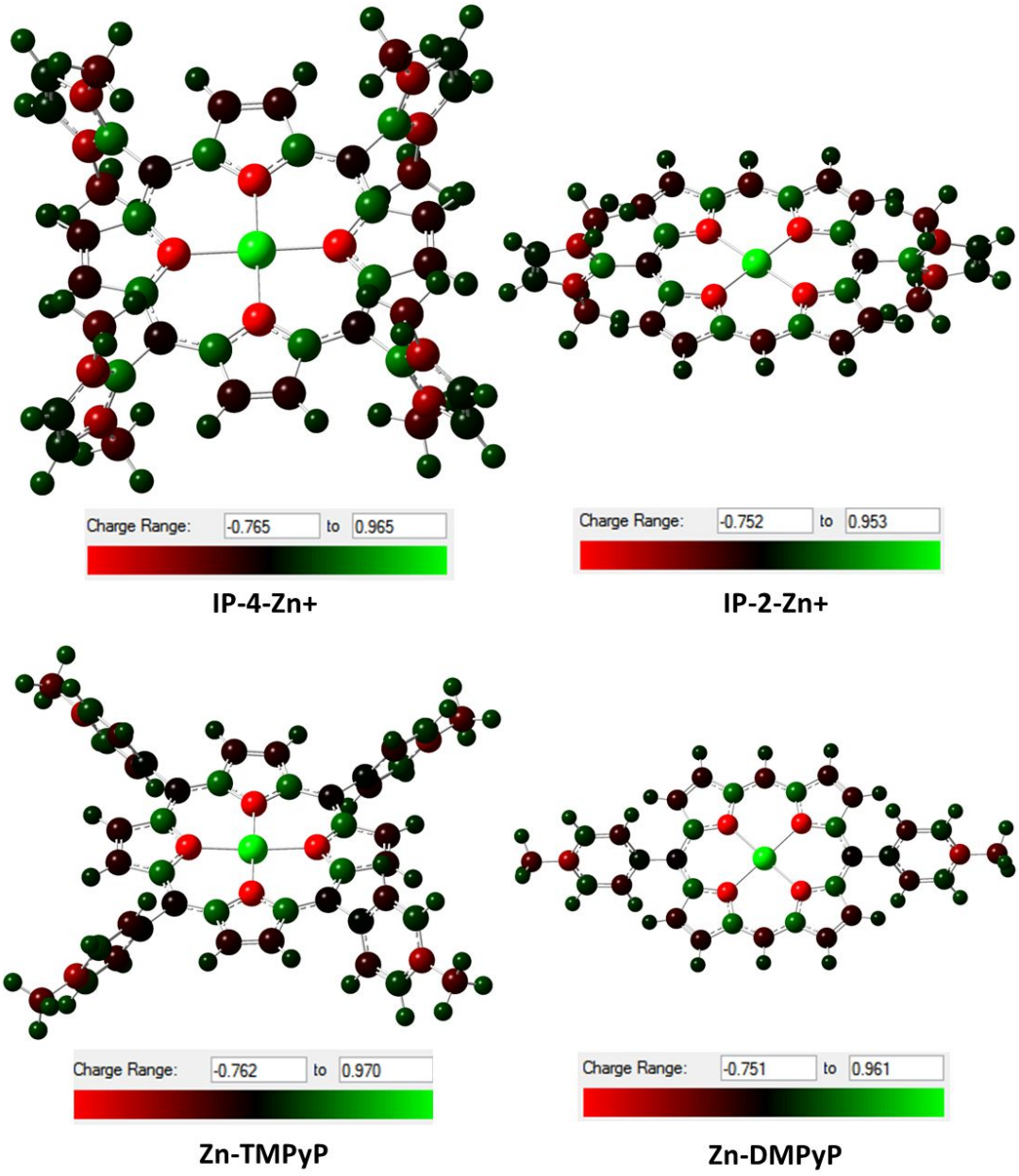

Figure S4. Mulliken charges of zinc complexes of cationic porphyrins optimized at the B3LYP/6-31G(d,p) level.

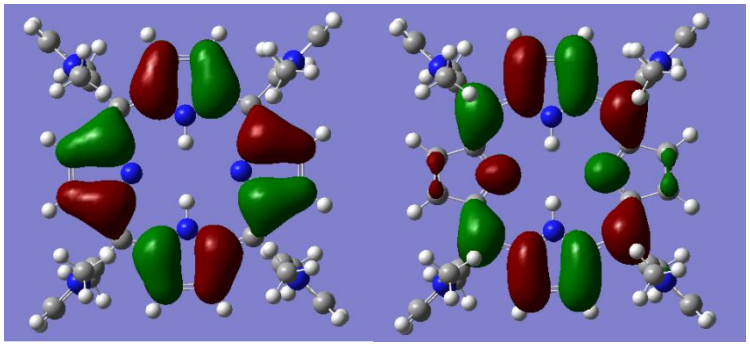

IP-4-H+, ΔE(HOMO–LUMO) = 2.79 eV

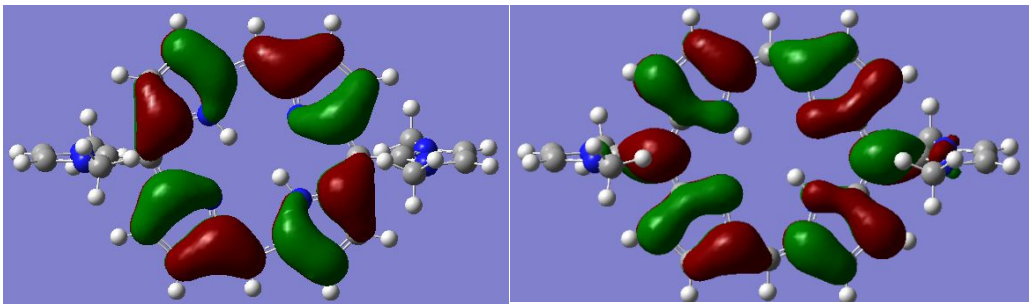

IP-2-H+, ΔE(HOMO–LUMO) = 2.70 eV

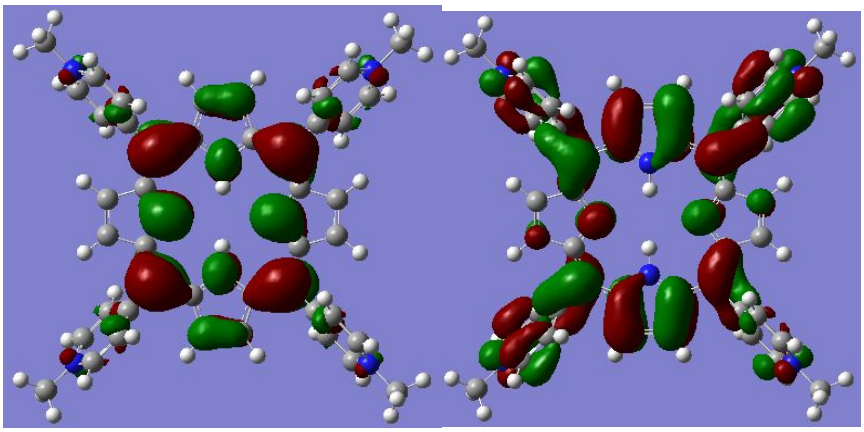

TMPyP, ΔE(HOMO–LUMO) = 2.63 eV

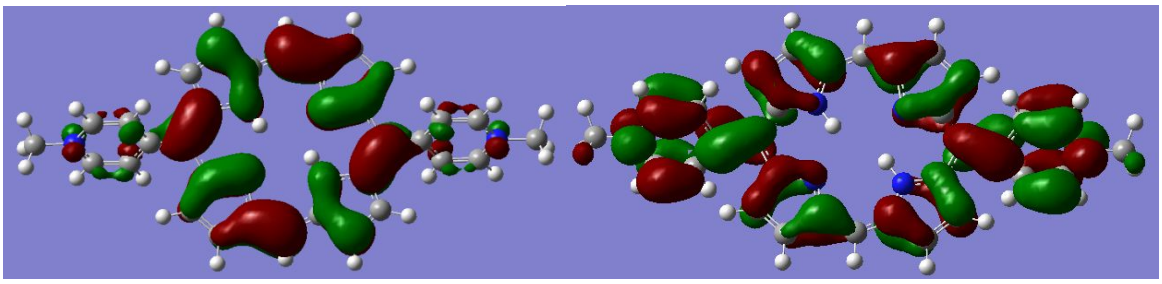

DMPyP, ΔE(HOMO–LUMO) = 2.18 eV

Figure S5. HOMO and LUMO orbitals of free-base cationic porphyrins optimized at the B3LYP/6-31G(d,p) level.

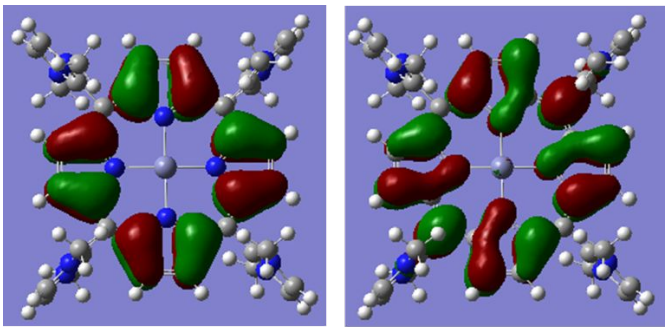

HOMO LUMO

IP-4-Zn+, ΔE(HOMO–LUMO) = 2.83 eV

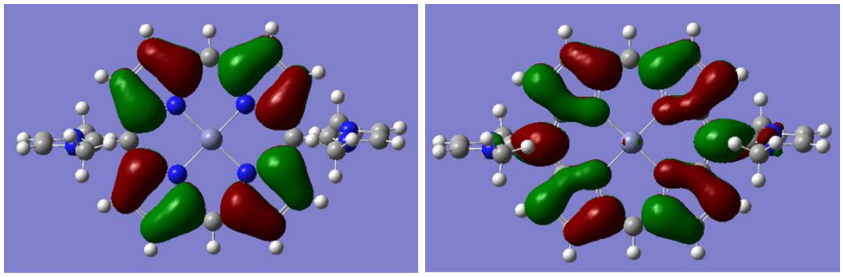

HOMO LUMO

IP-2-Zn+, ΔE(HOMO–LUMO) = 2.72 eV

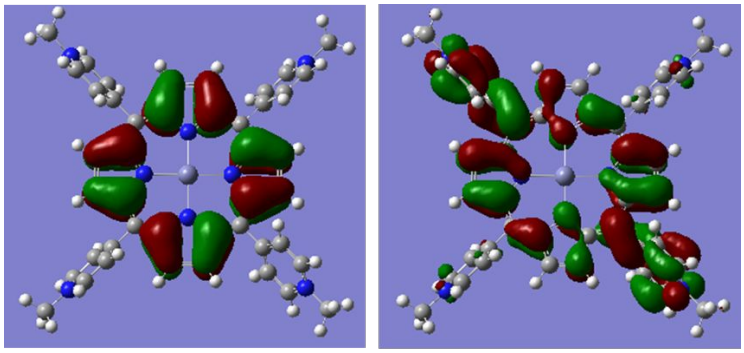

HOMO LUMO

Zn-TMPyP, ΔE(HOMO–LUMO) = 2.69 eV

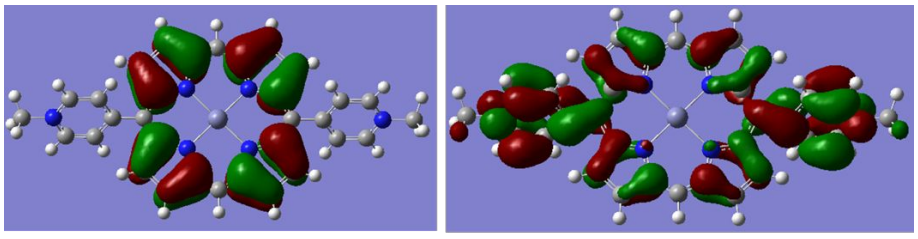

HOMO LUMO

Zn-DMPyP, ΔE(HOMO–LUMO) = 2.20 eV

Figure S6. HOMO and LUMO orbitals of zinc complexes of cationic porphyrins optimized at the B3LYP/6-31G(d,p) level.

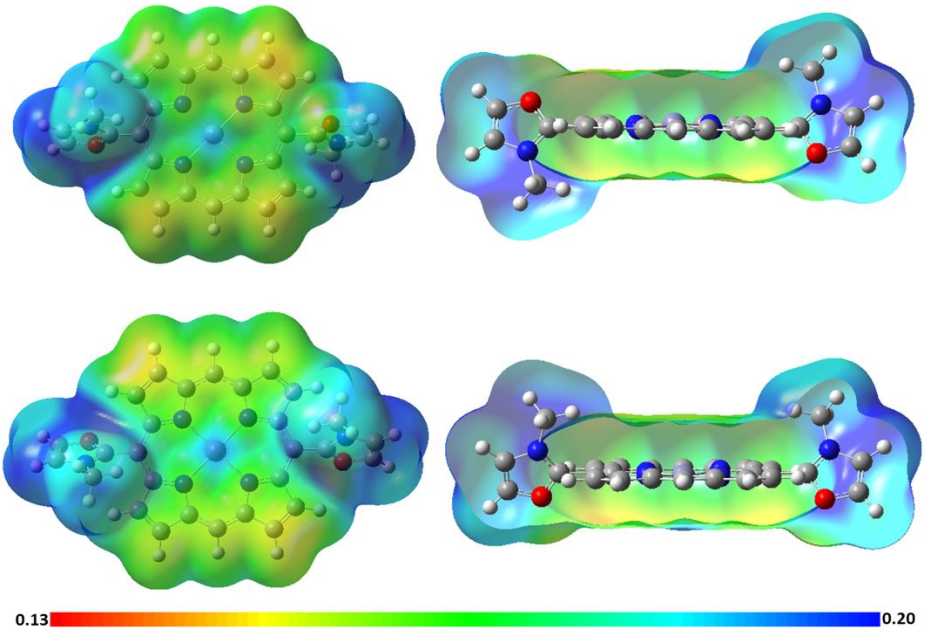

Figure S7. Electronic density of 5,15-bis(3-methyloxazol-2-yl)porphyrinate zinc (II) diiodide without their counterions, from total SCF density mapped with ESP, isovalue=0.0004.

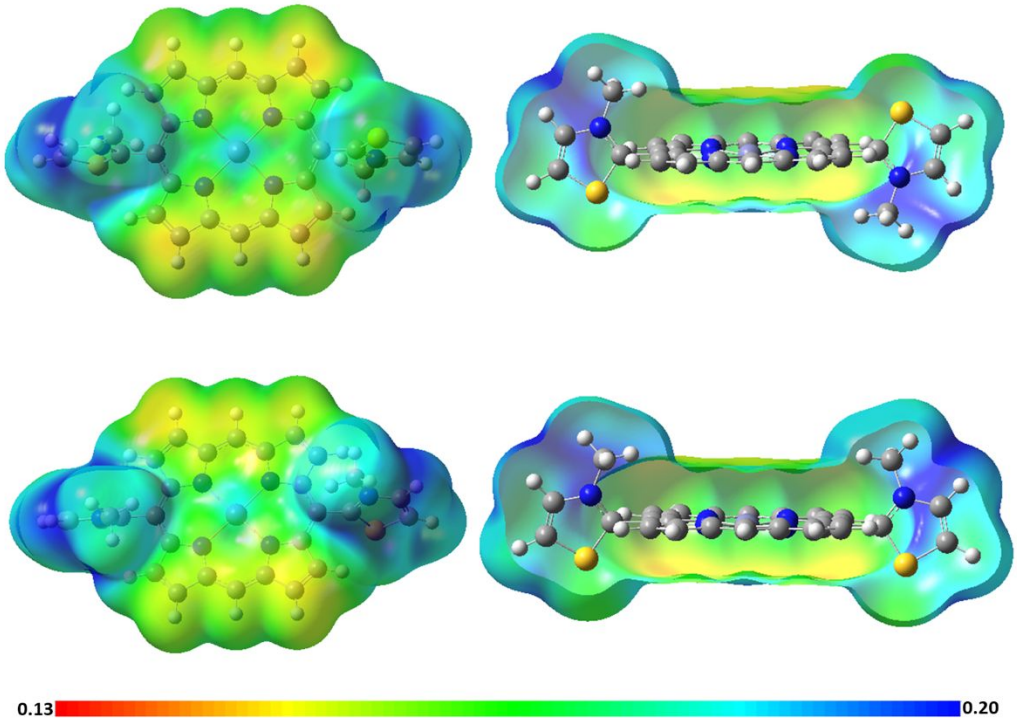

Figure S8. Electronic density of 5,15-bis(3-methylthiazol-2-yl)porphyrinate zinc (II) diiodide without their counterions, from total SCF density mapped with ESP, isovalue=0.0004.

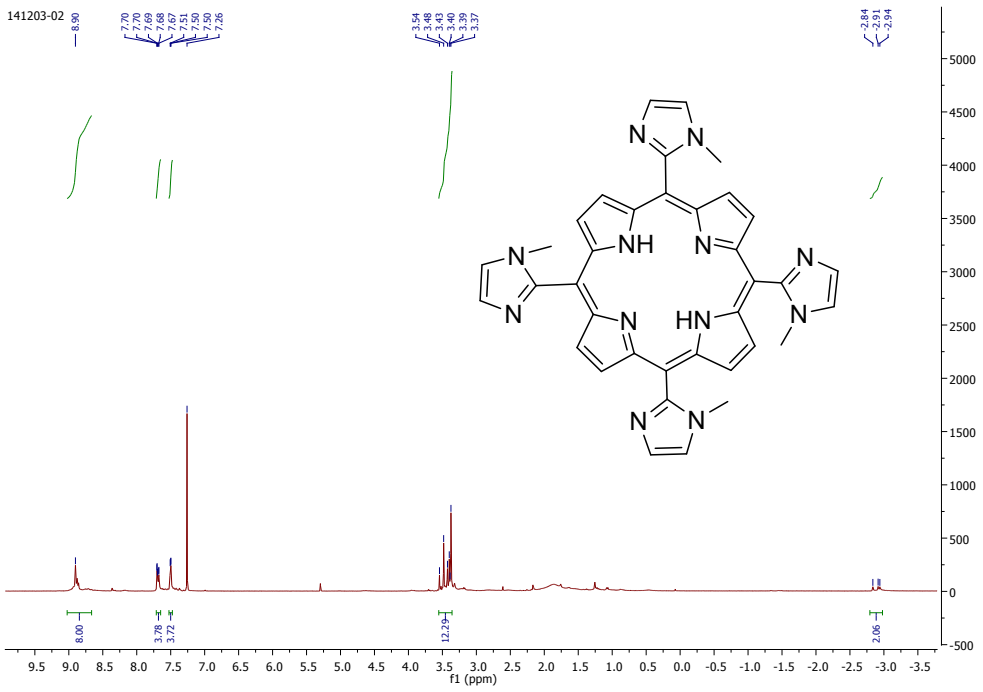

Figure S9. ^{1}H NMR Spectra of **IP-4-H** in deuterated chloroform.

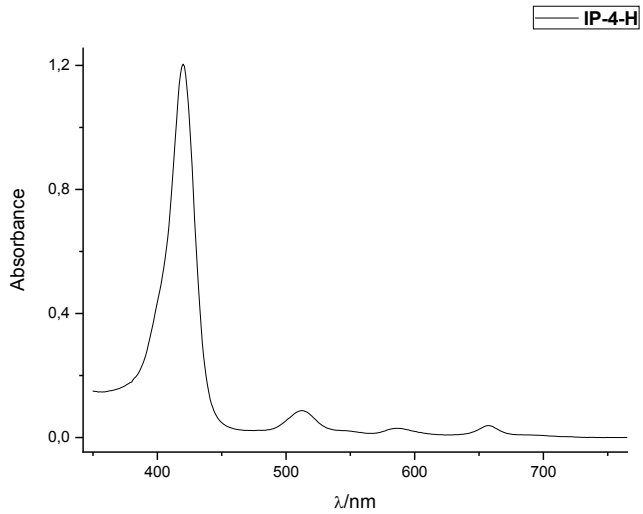

Figure S10. Normalized UV-vis spectra of **IP-4-H** in dichloromethane.

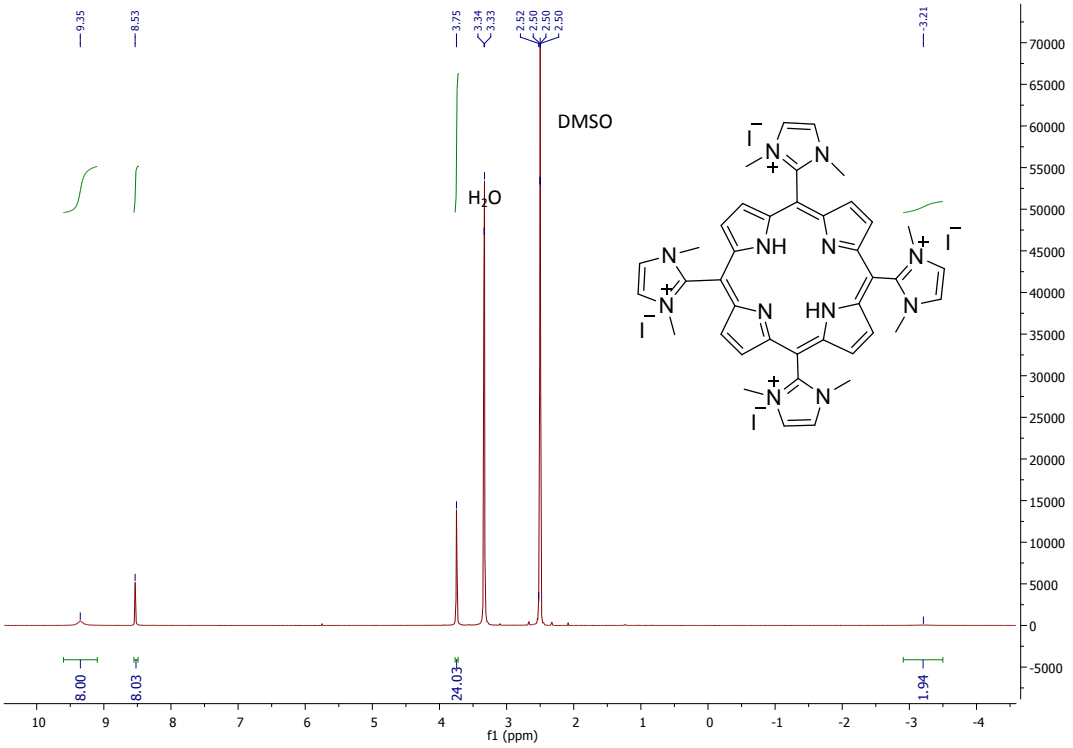

Figure S11. ^{1}H NMR Spectra of **IP-4-H+** in $(CD_3)_2SO$.

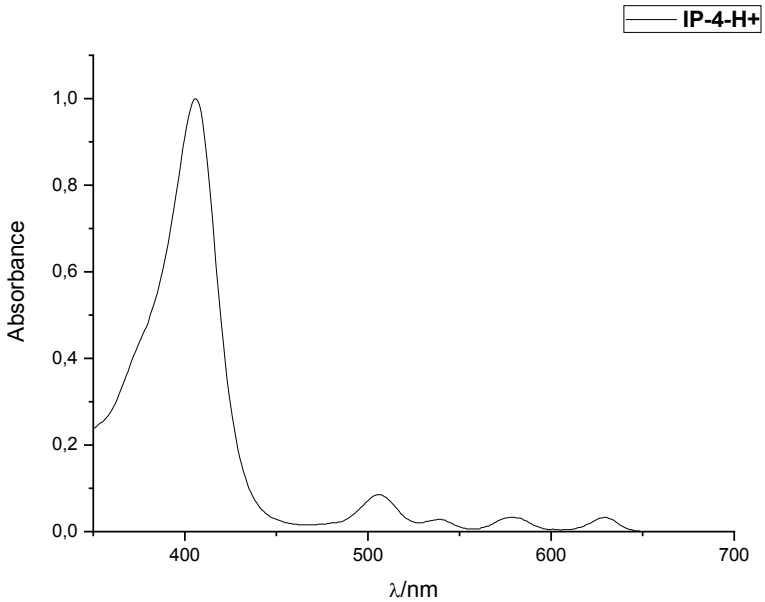

Figure S12. Normalized UV-vis spectra of **IP-4-H+** in water.

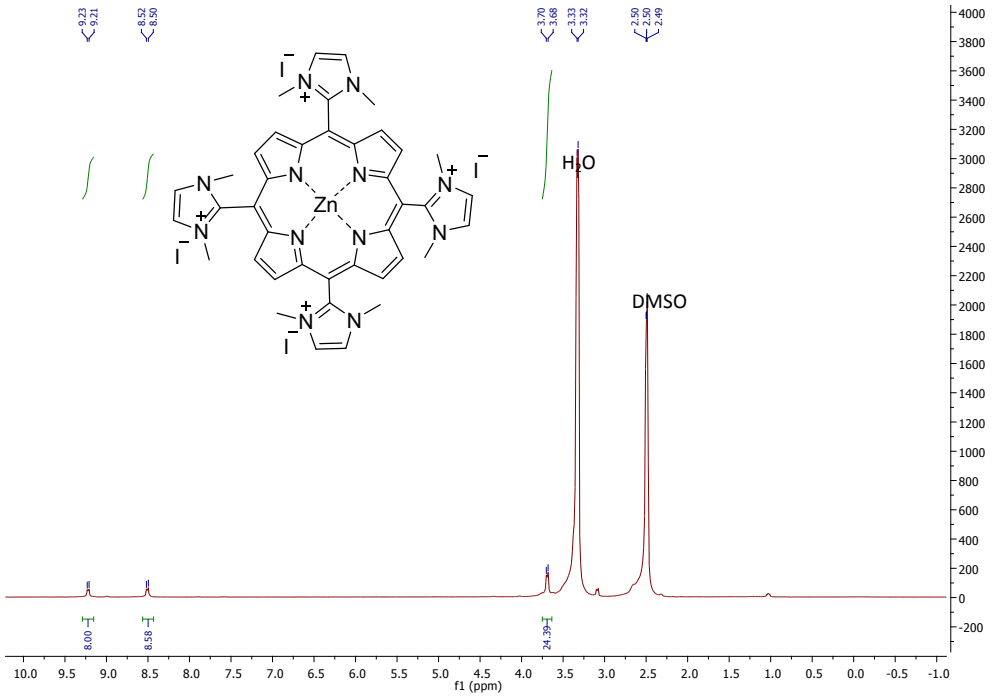

Figure S13. ^{1}H NMR Spectra of **IP-4-Zn+** in $(CD_3)_2SO$.

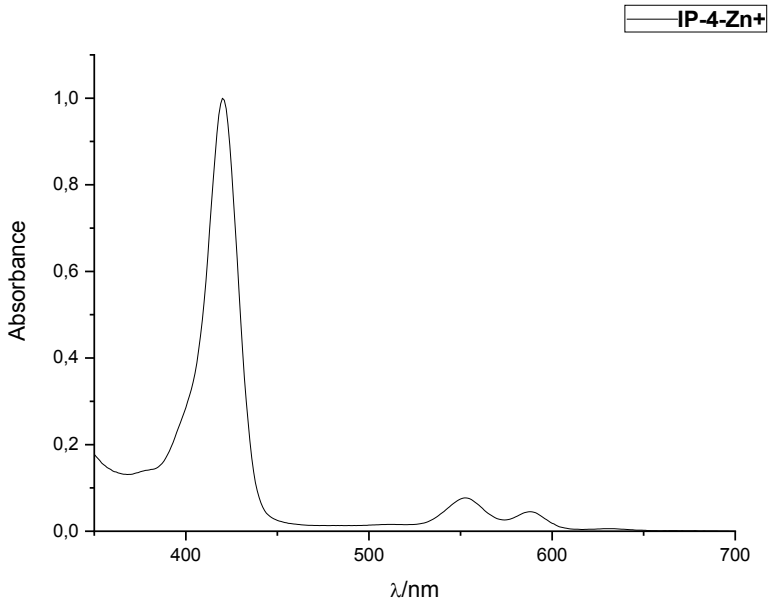

Figure S14. Normalized UV-vis spectra of **IP-4-Zn+** in water.

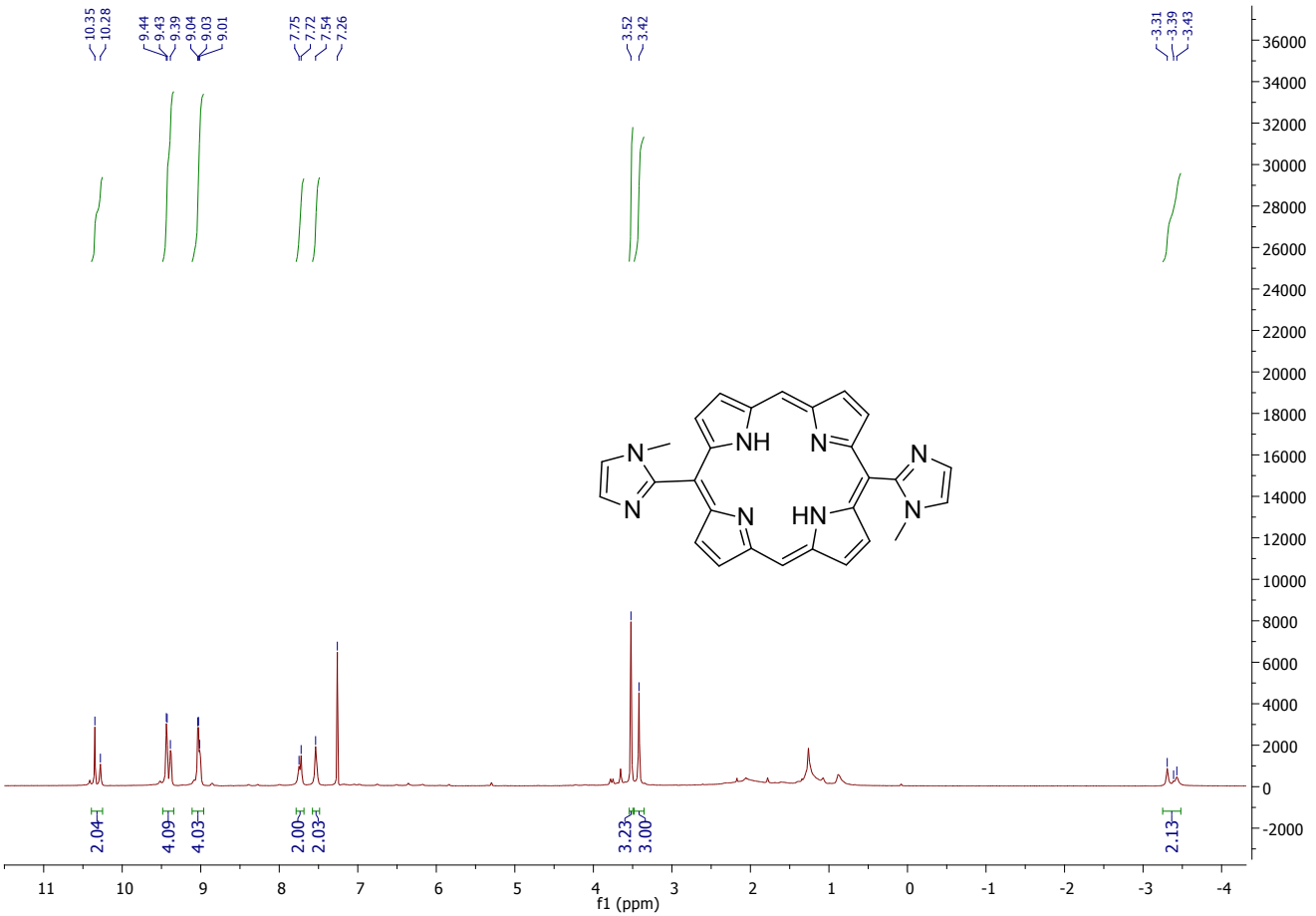

Figure S15. ^{1}H NMR Spectra of **IP-2-H** in deuterated chloroform.

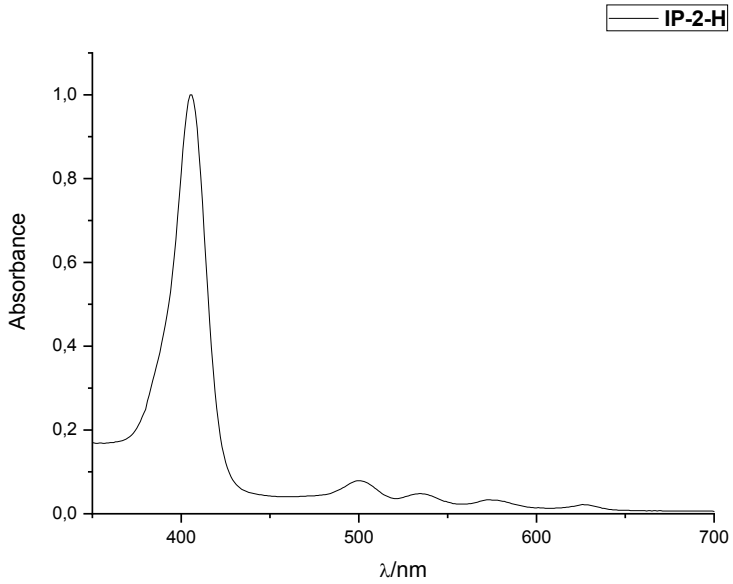

Figure S16. Normalized UV-vis spectra of **IP-2-H** in dichloromethane.

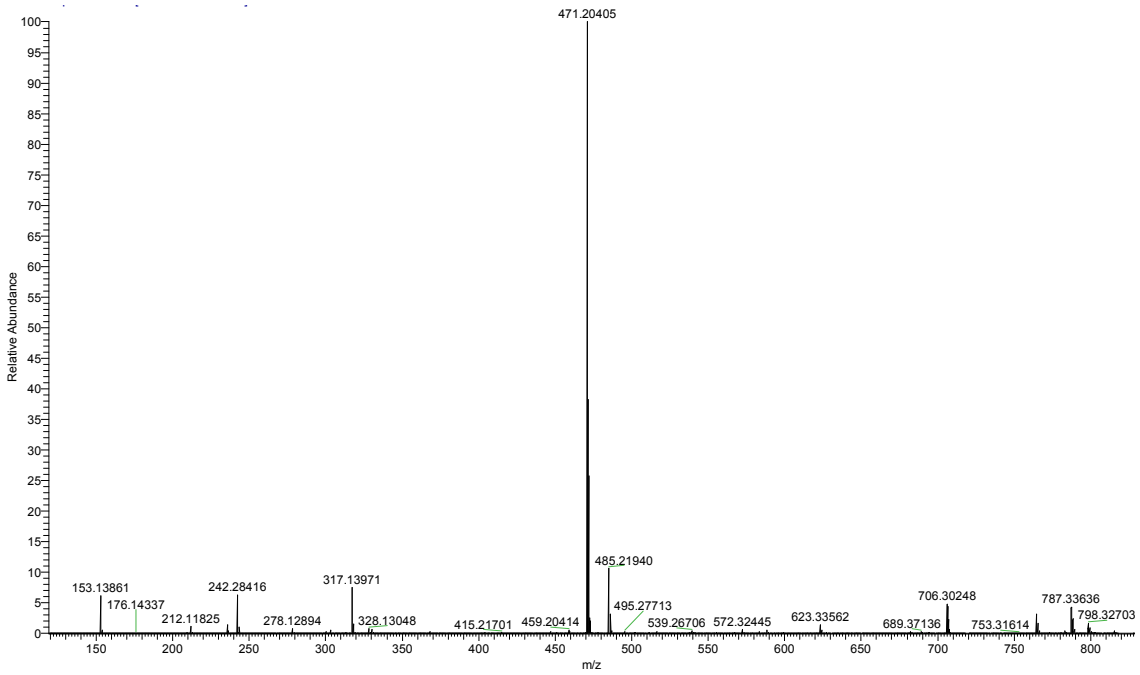

Figure S17. ESI mass spectrum of **IP-2-H** acquired in positive mode.

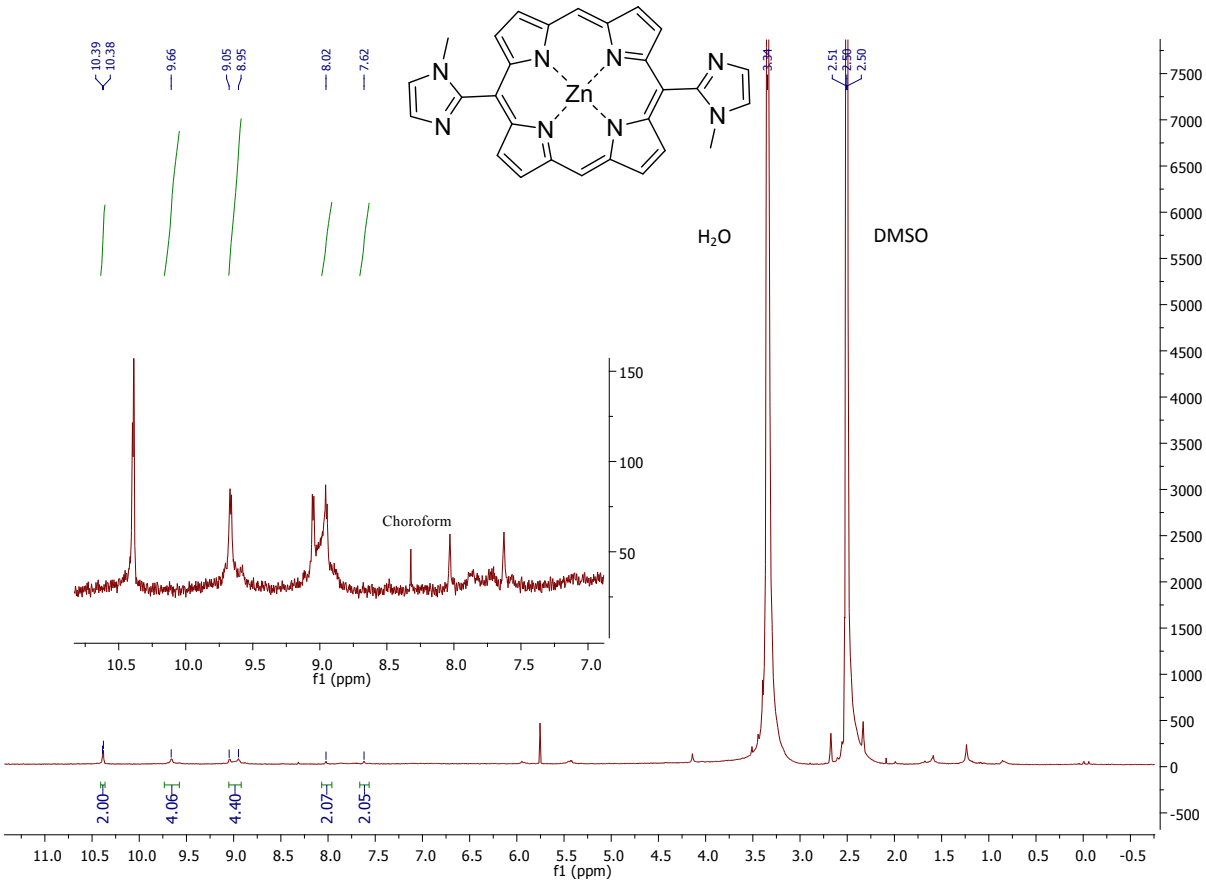

Figure S18. ^{1}H NMR Spectra of **IP-2-Zn** in $(CD_3)_2SO$.

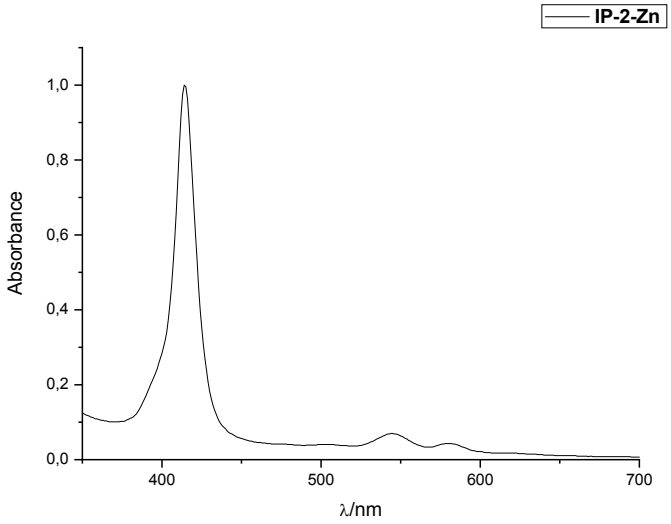

Figure S19. Normalized UV-vis spectra of **IP-2-Zn** in DMSO.

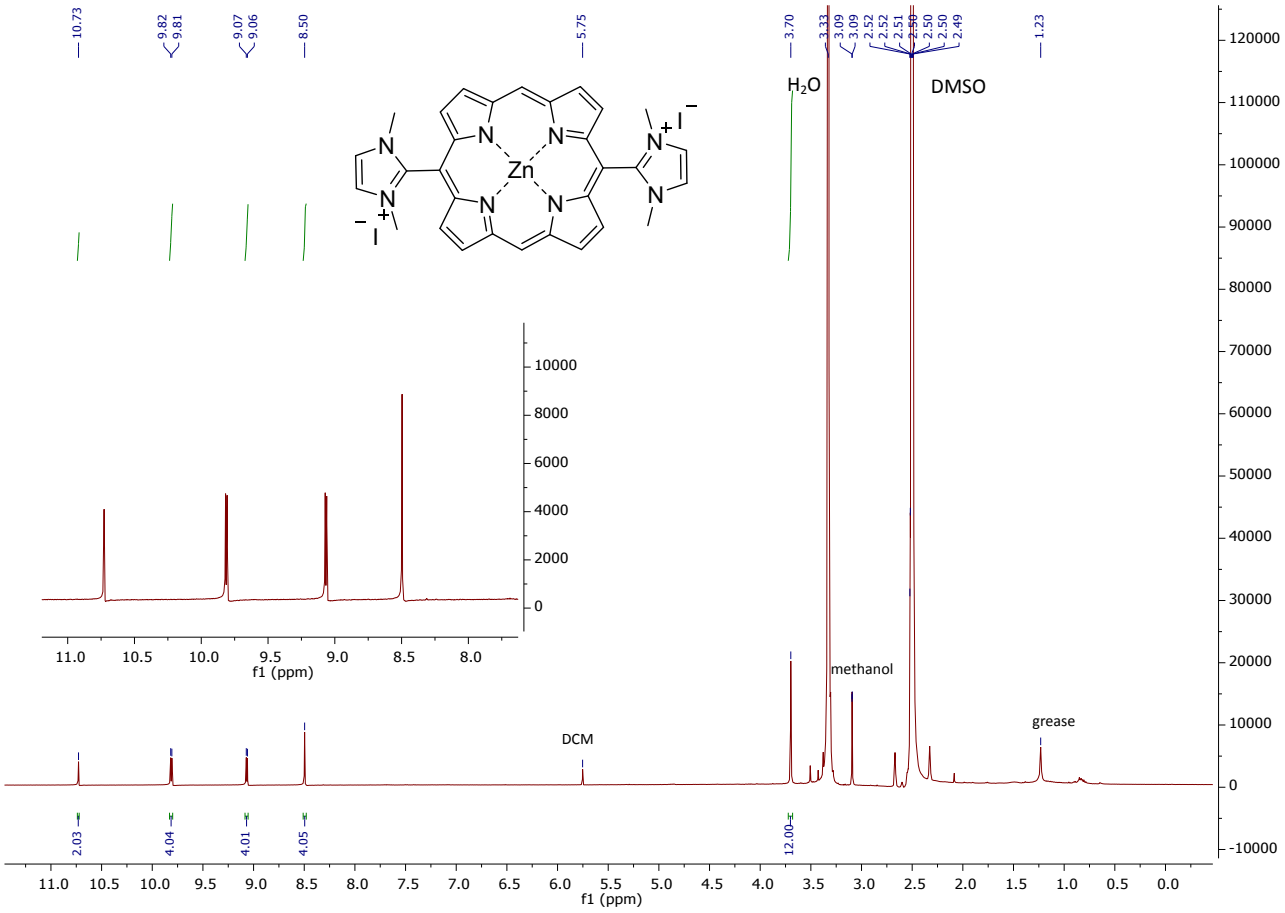

Figure S20. ^{1}H NMR Spectra of **IP-2-Zn+** in $(CD_3)_2SO$.

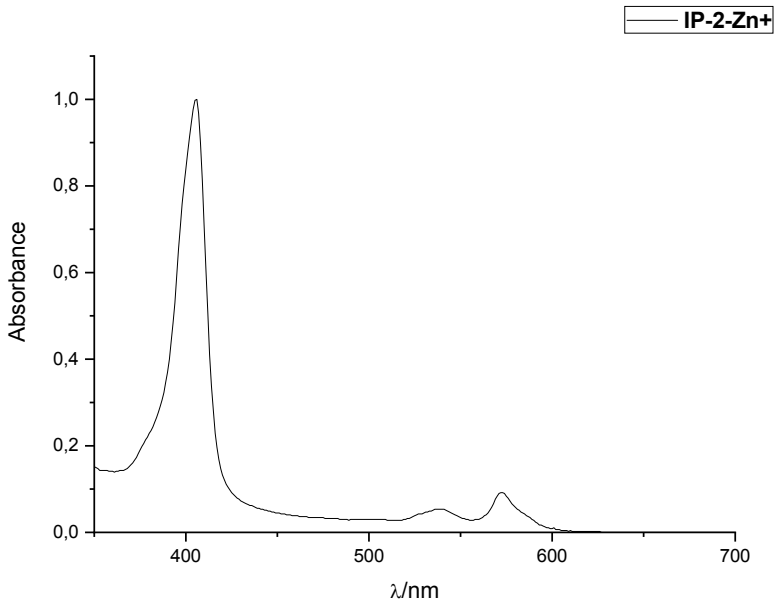

Figure S21. Normalized UV-vis spectra of **IP-2-Zn+** in water.

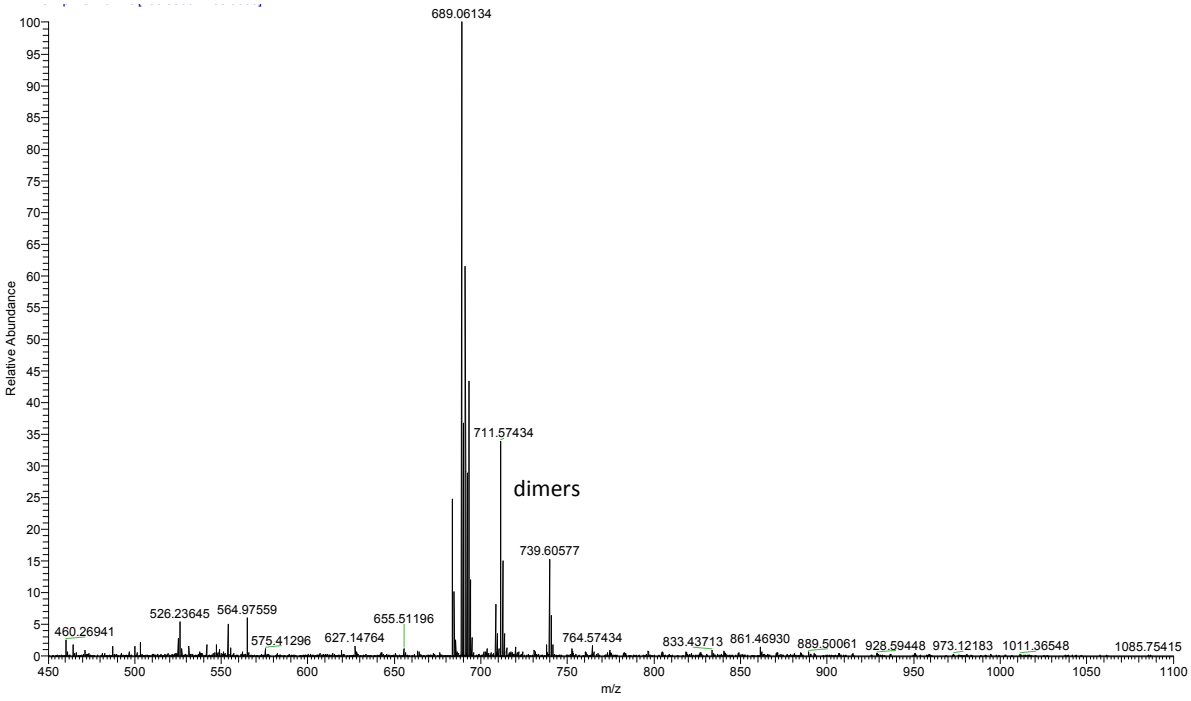

Figure S22. ESI mass spectrum of **IP-2-Zn+** acquired in positive mode.

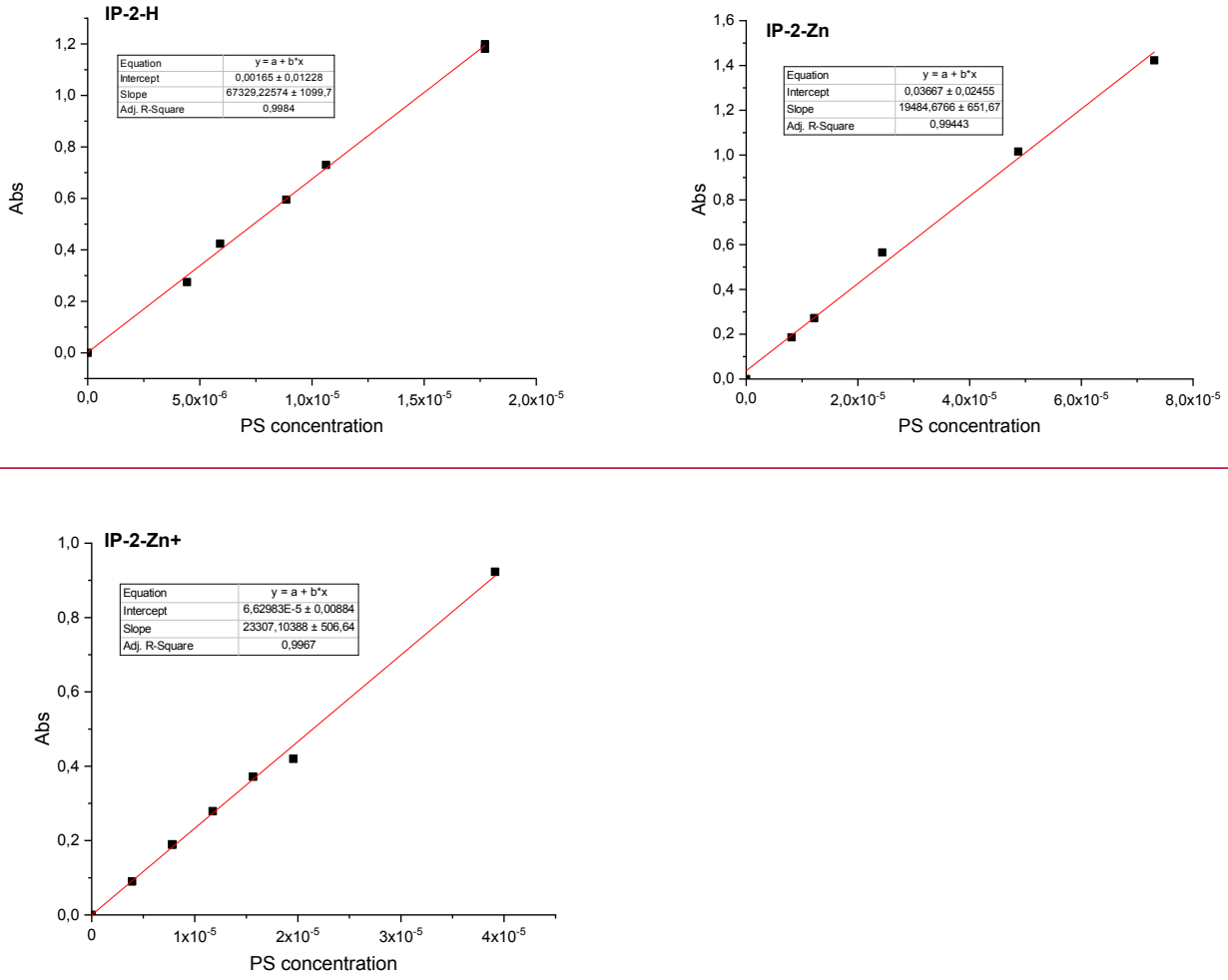

Figure S23. Absorption coefficient calculations for Soret band on PBS or PBS/DMSO (0,6%)

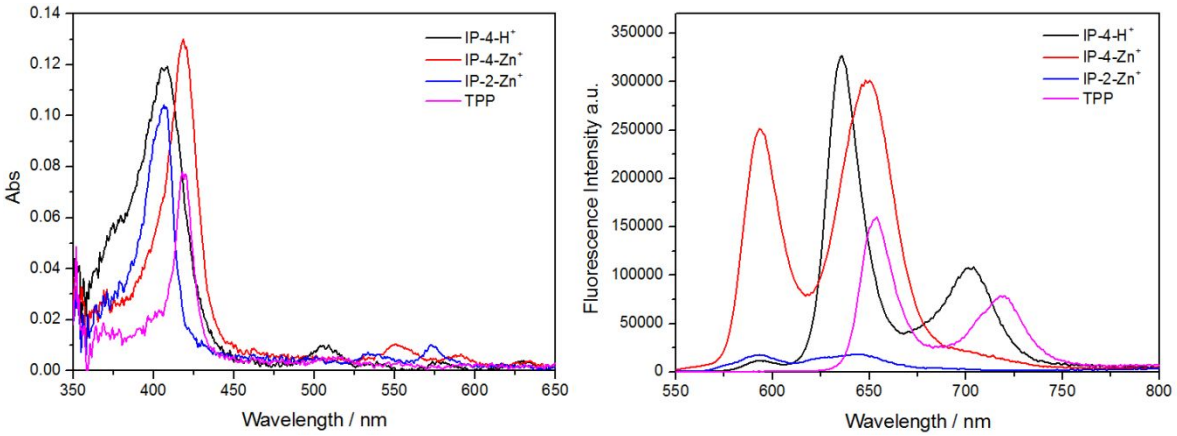

Figure S24. Absorption spectra (all solutions were diluted 10 times after recording the absorption spectra) and fluorescence spectra with excitation at 418nm for all samples.

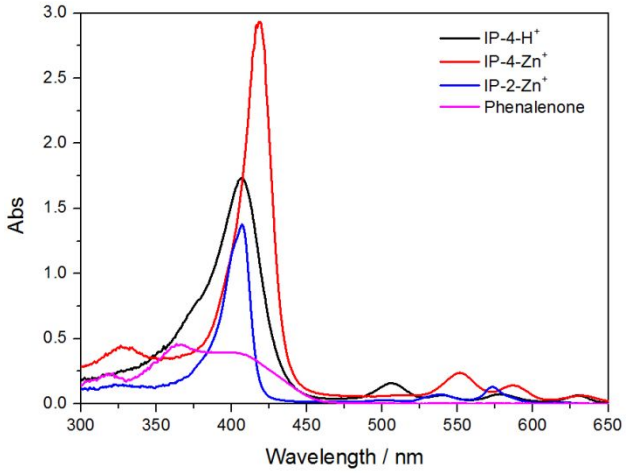

Figure S25. Electronic absorption spectra in D_2O (heavy water)

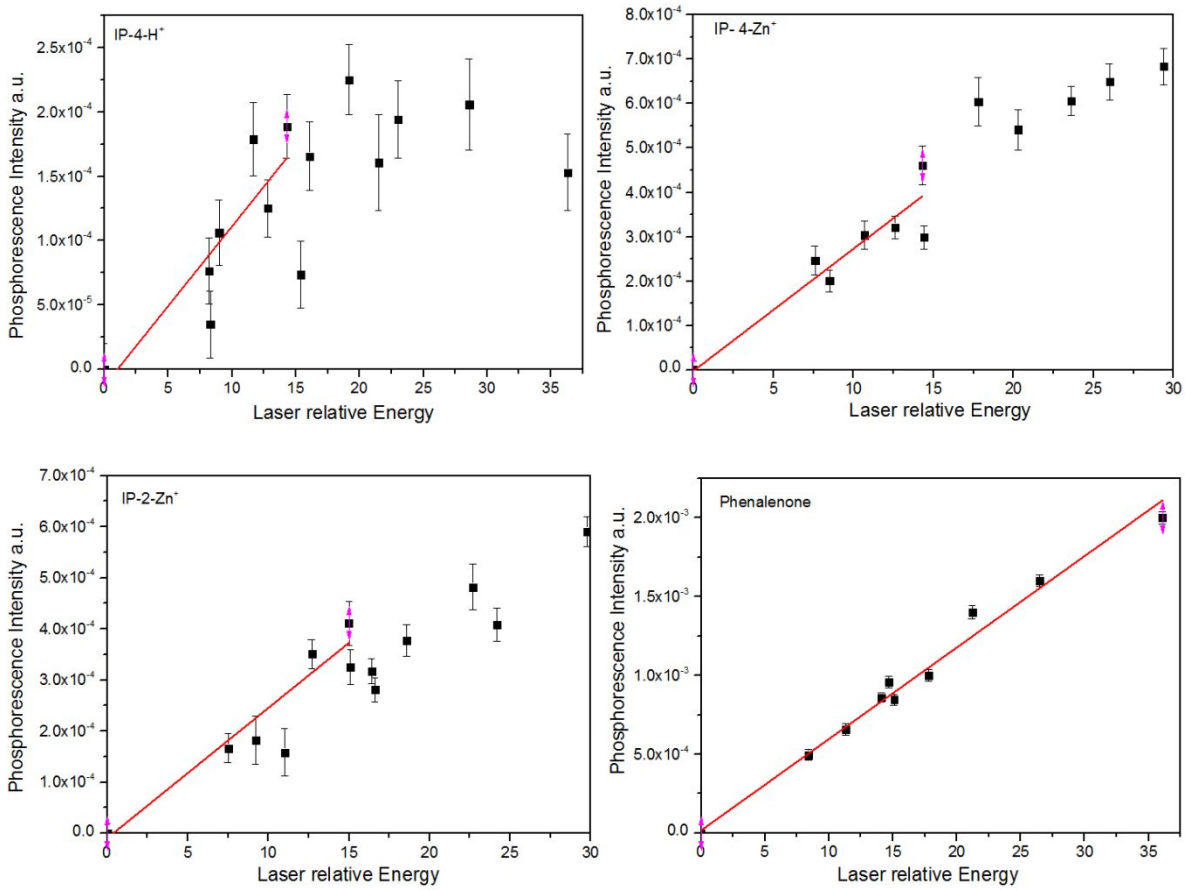

Figure S26. Pre-exponential values of singlet oxygen phosphorescence decays as a function of laser relative energy and corresponding linear fits. Excitation at 355 nm.

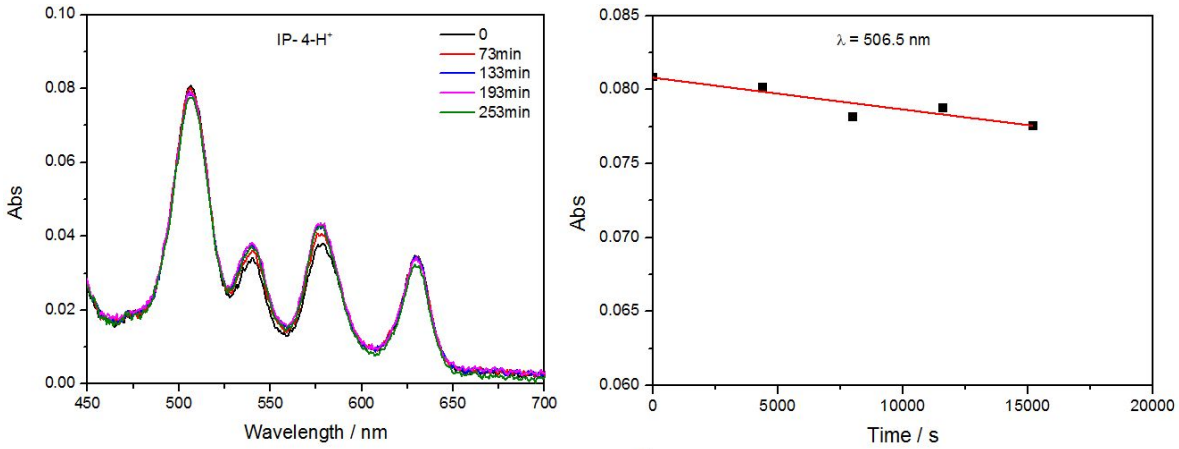

Figure S27. Photodecomposition of **IP-4-H**$^{+}$ with LED fluence of 0.81 mW/cm^2 (corrected for the light actually absorbed[9]).

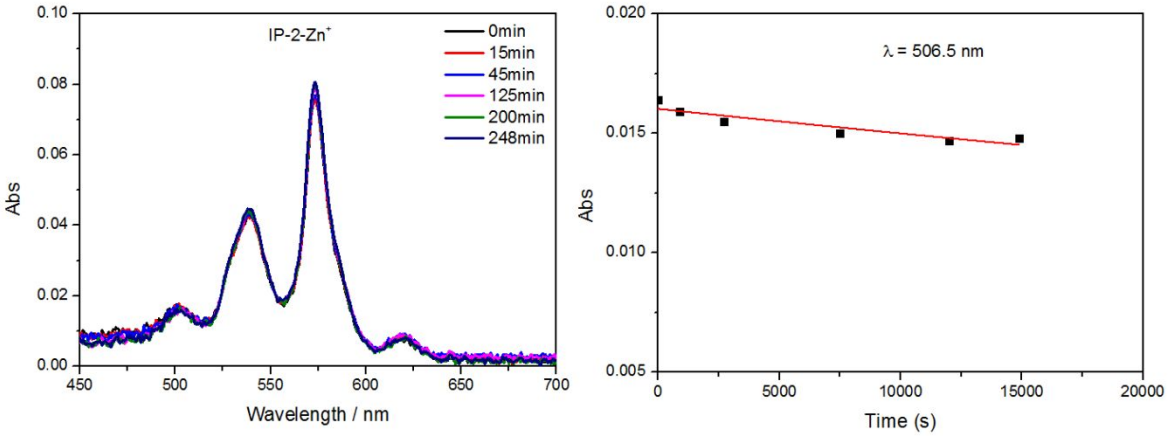

Figure S28. Photodecomposition of **IP-2-Zn+** with LED fluence of 0.54 mW/cm^2 (corrected for the light actually absorbed[9]).